RF Photonic Technology in Optical Fiber Links

Edited by **William S. Chang**

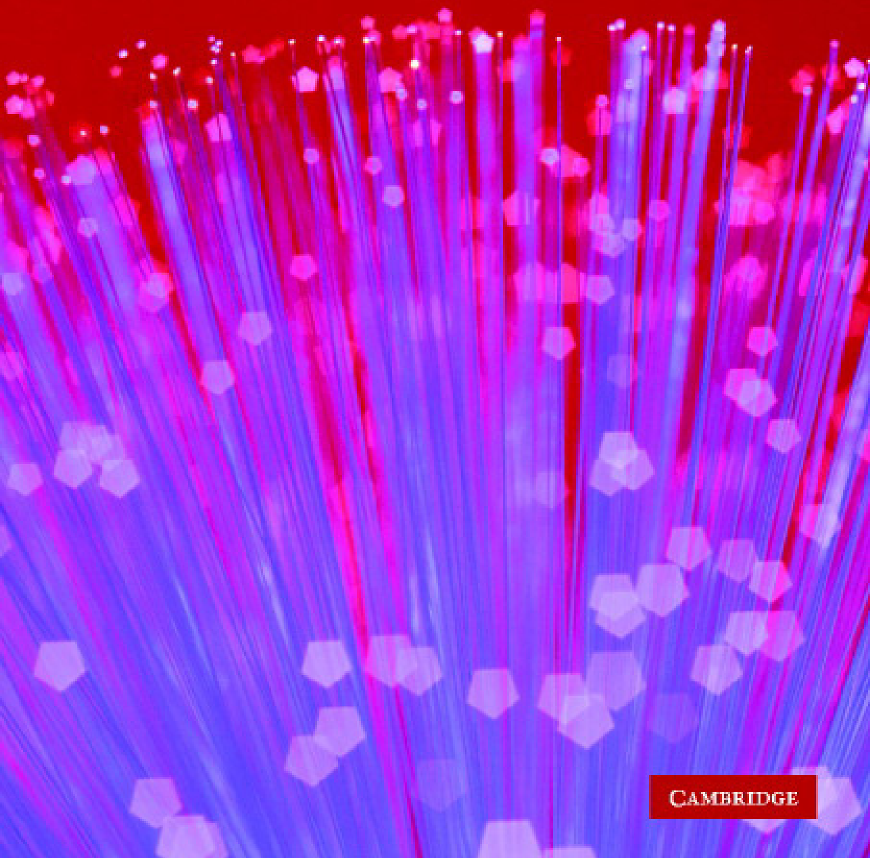

CAMBRIDGE

CAMBRIDGE

more information - www.cambridge.org/9780521803755

This page intentionally left blank

RF PHOTONIC TECHNOLOGY IN OPTICAL FIBER LINKS

In many applications, radio-frequency (RF) signals need to be transmitted and processed without being digitalized. These analog applications include CATV, antenna remoting, phased array antenna and radar amongst others. Optical fiber provides a transmission medium in which RF modulated optical carriers can be transmitted and distributed with very low loss. With modulation and demodulation of the optical carrier at the sending and receiving ends, the optical fiber system functions like a low-loss analog RF transmission, distribution, and signal processing system. RF photonic fiber technology has particular advantages in that it is more efficient, less complex, and less costly than conventional electronic systems, especially at high microwave and millimeter wave frequencies. Analog signal processing of RF signals can be achieved optically while the signal is being transmitted along the optical carrier. Examples of such processing techniques include up- and down-conversion of RF frequencies, true time delay of RF signals, and optical distribution of RF clocks.

This volume presents a review of RF photonic components, transmission systems, and signal processing examples in optical fibers from the leading academic, government, and industry scientists working in this field. It discusses important concepts such as RF efficiency, nonlinear distortion, spurious free dynamic range, and noise figures. This is followed by an introduction to various related technologies such as direct modulation of laser sources, external modulation techniques (including lithium niobate modulators, polymer modulators and semiconductor electroabsorption modulators), and detectors. In addition, several examples of RF photonic signal processing technology, such as the phased array, the optoelectronic oscillator, and up and down RF frequency conversion and mixing, are presented. These will stimulate new ideas for applications in RF photonic signal processing.

RF Photonic Technology in Optical Fiber Links will be a valuable reference source for professionals and academics engaged in the research and development of optical fibers and analog RF applications. The text is aimed at engineers and scientists with a graduate-school education in physics or engineering. With an emphasis on design, performance, and practical application, this book will be of particular interest to those developing novel systems based on this technology.

William Chang pioneered microwave laser and optical laser research at Stanford University between 1957 and 1959, whilst working as a lecturer and research associate. He subsequently joined the Ohio State University and established quantum electronic research there between 1959 and 1962. He became Professor and Chairman of the Electrical Engineering Department at Washington University, St. Louis in 1965, where he initiated research into guided wave and opto-electronic devices. In 1979 Professor Chang joined the University of California at San Diego and founded the well-known electronic device and materials group, as well as chairing the Department of Electrical and Computer Engineering from 1993 to 1996. He was made an Emeritus Professor of the department in 1997. Professor Chang has published more than 140 research papers on optical guided-wave research which in recent years have focused particularly on multiple quantum well electroabsorption modulators in III–V semiconductors.

RF PHOTONIC TECHNOLOGY IN OPTICAL FIBER LINKS

Edited by

WILLIAM S. C. CHANG
University of California, San Diego

CAMBRIDGE
UNIVERSITY PRESS

CAMBRIDGE UNIVERSITY PRESS
Cambridge, New York, Melbourne, Madrid, Cape Town, Singapore, São Paulo

Cambridge University Press
The Edinburgh Building, Cambridge CB2 2RU, United Kingdom

Published in the United States of America by Cambridge University Press, New York

www.cambridge.org

Information on this title: www.cambridge.org/9780521803755

First published in print format 2002

ISBN-13 978-0-511-05728-1 eBook (Adobe Reader)
ISBN-10 0-511-05728-8 eBook (Adobe Reader)

ISBN-13 978-0-521-80375-5 hardback
ISBN-10 0-521-80375-6 hardback

Contents

Contributors

Garry E. Betts
MIT Lincoln Laboratory
Lexington, MA 02173-9108, USA

John E. Bowers
Department of Electrical and Computer Engineering
University of California Santa Barbara
CA 93106, USA

William B. Bridges
California Institute of Technology
M/S 136-93, 1200 E. California Blvd.
Pasadena, CA 91125, USA

William K. Burns
Naval Research Laboratory
Washington DC, 20375-5000, USA

William S.C. Chang
Department of Electrical and Computer Engineering
University of California San Diego
La Jolla, CA 92093-0407, USA

Charles Cox
Research Laboratory of Electronics
Massachusetts Institute of Technology
Cambridge, MA, 02139, USA

Roger Helkey
Chromisys Corp.
25 Castilian Drive
Goleta, CA 93117, USA

Marta M. Howerton
Naval Research Laboratory
Washington DC, 20375-5000, USA

Ronald T. Logan
Phasebridge Inc.
859 S. Raymond Avenue
Pasadena, CA 91105, USA

Xiaolin Lu
Morning Forest, LLC
Highlands Ranch,
CO, USA

Willie Ng
HRL Laboratories, LLC
M/S RL64, 3011 Malibu Canyon Road
Malibu, CA 90265, US

Stephan A. Pappert
Lightwave Solutions, Inc.
8380 Miralani Drive, Suite B
San Diego, CA 92126-4347, USA

Joachim Piprek
Department of Electrical and Computer Engineering
University of California Santa Barbara
CA 93106, USA

Ron Stephens
HRL Laboratories, LLC
M/S RL64, 3011 Malibu Canyon Road
Malibu, CA 90265, US

Greg Tangonan
HRL Laboratories, LLC
M/S RL64, 3011 Malibu Canyon Road
Malibu, CA 90265, US

Timothy Van Eck
Lockheed Martin Space Systems Company
3251 Hanover Street
Palo Alto, CA 94304, USA

Ming C. Wu
Department of Electrical Engineering
University of California Los Angeles
Los Angeles, CA 90095-1594

X. Steve Yao
General Photonics Corporation
5228 Edison Avenue,
Chino, CA 91710, USA

Daniel Yap
HRL Laboratories
M/S RL64, 3011 Malibu Canyon Road,
Malibu, CA 90265, US

Paul K. L. Yu
Department of Electrical and Computer Engineering
University of California San Diego
La Jolla, CA 92093-0407, USA

Introduction and preface

RF technology is at the heart of our information and electronic technology. Traditionally, RF signals are transmitted and distributed electronically, via electrical cables and waveguides. Optical fiber systems have now replaced electrical systems in telecommunications. In telecommunication, RF signals are digitalized, the on/off digitally modulated optical carriers are then transmitted and distributed via optical fibers. However, RF signals often need to be transmitted, distributed and processed, directly, without going through the digital encoding process. RF photonic technology provides such an alternative. It will transmit and distribute RF signals (including microwave and millimeter wave signals) at low cost, over long distance and at low attenuation.

RF photonic links contain, typically, optical carriers modulated, in an analog manner, by RF subcarriers. After transmission and distribution, these modulated optical carriers are detected and demodulated at a receiver in order to recover the RF signals. The transmission characteristics of RF photonic links must compete directly with traditional electrical transmission and distribution systems. Therefore the performance of an RF photonic transmission or distribution system should be evaluated in terms of its efficiency, dynamic range and its signal-to-noise ratio.

RF photonic links are attractive in three types of applications. (1) In commercial communication applications, hybrid fiber coax (HFC) systems, including both the broadcast and switched networks, provide the low cost network for distribution of RF signals to and from users. RF photonic technology has already replaced cables in commercial applications such as CATV. (2) At high frequencies, traditional microwave and millimeter wave transmission systems, using coaxial cables and metallic waveguides, have extremely large attenuation. Electrical systems are also complex and expensive. Other advantages of RF photonic methods include small weight and size, and immunity to electromagnetic disturbances. RF photonic systems offer an attractive alternative to traditional electrical systems at high frequencies. However, much of the RF technology for high frequency application is still in the research and development stage. It is important to understand the operation of each new development and to assess the implication of each new component before any application of the photonic link. (3) Once the RF signal is carried on an optical carrier, photonic techniques may be used to process the RF signals. An obvious example is the frequency up- or down- conversion of the RF signal. Therefore, photonic RF signal processing represents a potential attractive application area for new applications. However, in photonic RF signal processing, the system performance will have additional requirements than just the requirements for bandwidth, efficiency and dynamic range. For example, the phase noise of the RF signal becomes an important consideration in sensor applications.

System design consideration and the choice of the technologies and components to be used in RF photonic links, as well as the evaluation of their performance characteristics, are very different for analog links than for digital optical fiber links. For example, the "on–off" threshold switching voltage of a modulator is important for digital communication systems while the slope efficiency is the important figure of merit for analog modulation. A thorough understanding of the analog system issues and component requirements is necessary for a successful system design.

This monograph describes, in detail, the various key components and technologies that are important in analog RF links. The components are evaluated in terms of their potential contributions to the RF links, such as RF efficiency, bandwidth, dynamic range and signal-to-noise ratio. Since the modulation of an optical carrier is much smaller than its bias for analog links, a special feature of the analyses presented in this book is the use of small signal approximations with emphasis on the reduction of nonlinear distortions.

The objectives of this book are: (1) to present to the reader various key technologies that may be used in RF photonic links: (2) to assess the significant aspects of various technologies; (3) to explore extant and potential applications of such technologies; (4) to illustrate specific applications of RF photonic links.

The analyses of basic RF photonic links are presented in Chapter 1. The analyses show clearly the important figures of merit of various components and the system objectives of analog RF photonic links. Chapter 2 describes the role of RF subcarrier links in commercial local access networks. Modulation and detection techniques are of particular importance in RF photonic links, because they determine the nonlinear distortion, the bandwidth, the efficiency, and, in certain cases, the noise of such links. Chapters 3 to 7 describe various modulation techniques, including the direct modulation of semiconductor lasers, the $LiNbO_3$ external modulators, the traveling wave modulator, the polymer modulator and the electroabsorption semiconductor modulator. The basic materials and principles of operation, the performance expectation and the advantages and limitations of each modulation technique are presented. In Chapter 8, a description of the key features of various detectors is presented. In the next three chapters, Chapters 9 to 11, three novel techniques, photonic frequency up- and down-conversion, integration of antenna and modulators at high millimeter wave frequency and optical generation of high RF frequency oscillation are discussed. They may offer hitherto unavailable opportunities for applications of RF photonic technology. Since RF modulation of optical carriers can be transmitted via fibers over long distance and with true delay, RF photonic technology can be used for antenna remoting and RF signal processing. Chapter 12 illustrates an important application of RF photonic technique to antenna remoting and to the phased array antennas.

University of California, San Diego *William S. C. Chang*

1

Figures of merit and performance analysis of photonic microwave links

CHARLES COX

MIT, Cambridge, MA

WILLIAM S. C. CHANG

University of California, San Diego

1.1 Introduction

Microwave links serve important communication, signal processing and radar functions in many commerical and military applications. However, the attenuation of microwave RF signals in cables and waveguides increases rapidly as the frequency of the signal increases, and it is specially high in the millimeter wave range. Optical fibers offer the potential for avoiding these limitations for the transmission of RF signals.

Photonic microwave links employ optical carriers that are intensity modulated by the microwave signals[1] and transmitted or distributed to optical receivers via optical fibers. Since the optical loss for fibers is very low, the distance for photonic transmission and distribution of microwaves can be very long. When the modulation of an optical carrier is detected at a receiver, the RF signal is regenerated. Figure 1.1 illustrates the basic components of a simple photonic microwave link.

Since the objective of a photonic microwave link is to reproduce the RF signal at the receiver, the link can convey a wide variety of signal formats. In some applications the RF signal is an unmodulated carrier – as for example in the distribution of local oscillator signals in a radar or communication system. In other applications the RF signal consists of a carrier modulated with an analog or digital signal.

From the point of view of input and output ports, photonic microwave links function just like conventional microwave links. A common example is to transmit or to distribute microwave signals to or from remotely located transmitting or receiving antennas via optical fibers. Another common example is to distribute cable TV signals via optical fibers. Not only RF signals can be transmitted in this manner; microwave functions such as mixing (up-conversion or down-conversion) of signal frequencies can also be carried out photonically. We will discuss the

[1] Intensity modulation is in universal use today. Modulation of other parameters of the optical wave, such as its frequency, is in the research stage.

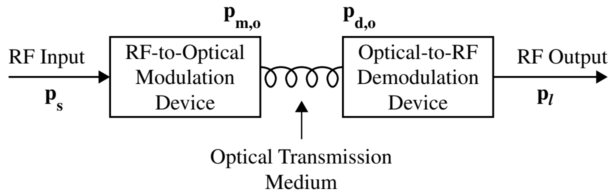

Figure 1.1. Basic components of a fiber optic link: modulation device, optical fiber and photodetection device.

figures of merit and performance measures of photonic RF transmission links in this chapter. The details of devices for the conversion between the RF and optical domains are discussed in other chapters of this book.

The objective of RF photonic links is clearly to achieve the same functions as conventional microwave links with longer distance of transmission, reduced cost, better performance, higher operating frequency, or reduced complexity and size. For this reason, their performance will be evaluated in terms of the criteria for microwave links. For microwave links – which are passive – typical performance criteria include just RF loss and frequency response. There is no nonlinear distortion or additional noise unless the signal is amplified. In photonic microwave links however, additional noise, such as the laser noise, can degrade the noise figure, and nonlinearity of the modulation process can reduce the spurious free dynamic range. Therefore, for microwave transmission and distribution using photonic links, which are more like active RF components, the important performance criteria are: (1) the RF gain and frequency response, (2) the noise figure (*NF*), and (3) the spurious free dynamic range (*SFDR*). These topics will be discussed in Sections 1.2, 1.3, and 1.4, respectively. For systems involving frequency mixing the figures of merit and the performance will be discussed in chapters presenting these techniques.

From the optical point of view, the magnitude of the RF intensity modulation is much less than the intensity of the unmodulated optical carrier. For this reason, one can analyze the link in the small signal approximation. Consequently, at a given DC bias operation point, the time variation of the optical intensity can be expressed as a Taylor series expansion about this DC bias point as a function of the RF signal magnitude.

To demonstrate clearly the system impact of such photonic link parameters as the CW optical carrier intensity, the noise, and the nonlinear distortion, we have chosen to discuss in this chapter the properties of just an *intrinsic* RF photonic link. In an intrinsic link no electronic or optical amplification is employed. An RF signal, at frequency ω, is applied to a modulation device to create intensity modulation of an optical carrier. The modulated carrier is transmitted to the receiver by a single fiber. The RF signals generated by the photodetector receiver constitute the RF output of the link. Only direct detection of the optical intensity (without amplification or any noise compensation scheme such as coherent detection) is considered for our discussion. Distribution of the optical carrier is limited to a single optical receiver. RF gain, *NF* and *SFDR* of such a basic link are analyzed in this chapter. Analysis of complex links involving amplification, distribution, and schemes for noise or distortion reduction, can be extended from the analysis of the intrinsic link.

There are two commonly used methods to create an RF intensity modulation of the CW optical carrier; one is by direct RF modulation of the laser and the second one is by RF modulation of the CW optical carrier via an external modulator. When the distinction between these two modulation methods is not germane to the discussion, we refer to them collectively as the modulation device. The RF gain, the *NF*, and the *SFDR* for both methods are discussed here.

1.2 Gain and frequency response

Conversion efficiencies, especially of the modulation device, are typically less than 10%, which leads immediately to photonic link losses of greater than 20 dB! This situation has motivated considerable work on efficiency improvement techniques. Conceptually there are two routes one can pursue: (1) improve the modulation device, and (2) improve the circuit that interfaces the modulation signal source to the modulation device. In this chapter we set up the analytical framework that shows how each of these approaches affects the solution. We also present an introductory investigation of how the interface circuit can improve performance.

The linear RF gain (or loss) of the link, g_{t}, is defined as the ratio of "the RF power, p_{l}, at frequency ω delivered to a matched load at the photodetector output" to "the available RF power at the input, p_{s}, at a single frequency ω and delivered to the modulation device." That is,

$$g_{\mathrm{t}} = \frac{p_{\mathrm{l}}}{p_{\mathrm{s}}}. \tag{1.1}$$

Frequently the RF gain is expressed in the dB scale as G_{t}, where $G_{\mathrm{t}} = 10\log_{10} g_{\mathrm{t}}$. If G_{t} is negative, it represents a loss.

The RF gain of a photonic link is frequency dependent. For links using simple input and output electrical circuits consisting of resistances and capacitances, their RF gain generally decreases as the frequency is increased. To quantify the *low pass* frequency response, the RF bandwidth f_{B} is defined as the frequency range from its peak value at DC to the frequency at which G_{t} drops by 3 dB. For a *bandpass* frequency response, which requires a more complex driving circuit, the G_{t} peaks at a center frequency. In this case, the bandwidth is the frequency range around the center frequency within which G_{t} drops less than 3 dB from its peak value.

There are three major causes of frequency dependence. (1) The directly modulated laser or the external modulator for the CW laser may have frequency dependent characteristics. (2) The voltage or current delivered to the modulation device may vary as a function of frequency due to the electrical characteristics of the input circuit. (3) The receiver and the detector may have frequency dependent responses.

Let $p_{\mathrm{m,o}}$ be the rms magnitude of the time varying optical power at frequency ω (immediately after the modulation device) in the fiber. Let $p_{\mathrm{d,o}}$ be the rms magnitude of the optical power at ω incident on the detector. Here, the subscript o denotes optical quantities, subscript m designates modulated optical carrier at ω at the beginning of the fiber and subscript d designates modulated optical carrier at ω incident on the detector. Quantities that do not have the o subscript apply to the RF. Then

$$p_{\mathrm{d,o}} = T_{\mathrm{M-D}}\, p_{\mathrm{m,o}}, \tag{1.2}$$

where $T_{\mathrm{M-D}}$ is the total optical loss incurred when transmitting the optical modulation from the modulation device to the detector. This quantity includes the propagation loss of the fiber and the coupling loss to and from the fiber. Since $p_{\mathrm{m,o}}$ is proportional to the current or the voltage of the RF input, $p^2_{\mathrm{m,o}}$ is proportional to p_{s}. Since the RF photocurrent at ω generated by the detector is proportional to $p_{\mathrm{d,o}}$ and since the RF power at the link output is proportional to the square of the photocurrent, $p^2_{\mathrm{d,o}}$ is proportional to p_{load}. Substituting the above relations into Eqs. (1.1) and (1.2) we obtain:

$$g_{\mathrm{t}} = \left(\frac{p^2_{\mathrm{m,o}}}{p_{\mathrm{s}}}\right) T^2_{\mathrm{M-D}} \left(\frac{p_{\mathrm{load}}}{p^2_{\mathrm{d,o}}}\right) \tag{1.3a}$$

or

$$G_{\mathrm{t}} = 10\log_{10}\left(\frac{p^2_{\mathrm{m,o}}}{p_{\mathrm{s}}}\right) + 20\log_{10} T_{\mathrm{M-D}} + 10\log_{10}\left(\frac{p_{\mathrm{load}}}{p^2_{\mathrm{d,o}}}\right). \tag{1.3b}$$

Strictly speaking, the definition of gain requires an impedance match between the modulation source and the modulation device. A typical RF source can be represented by a voltage source with rms voltage v_{s} at a frequency ω in series with an internal resistance R_{S}. As we will see below few, if any, modulation devices have an impedance equal to R_{S}. There are clearly myriad circuits that can accomplish the impedance matching function. The selection for any particular application depends upon many criteria – primary among them are cost, bandwidth and efficiency. We have chosen a few illustrative examples below; a more comprehensive discussion is included in the book by Cox [1].

The simplest – and least expensive – form of matching is to use a resistor. However a resistor is a lossy device, so this form of matching is not very efficient. Thus lossless impedance matching (an ideal situation that can only be approximated in practice) offers greater efficiency but at increased circuit complexity, and hence cost. We will present one example from both categories in the discussion below.

As will become clearer in the sections to follow, $p_{\mathrm{m,o}}^2/p_{\mathrm{s}}$ is an important figure of merit because it contains the combined effects of the modulation device impedance and slope efficiency. To get a feel for $p_{\mathrm{m,o}}^2/p_{\mathrm{s}}$, we will present explicit formulations for several representative cases. In each case we will need to derive two expressions: one for the relationship between the modulation source power, p_{s}, and the modulation voltage or current; and one relating the modulation voltage or current to the modulated optical power, $p_{\mathrm{m,o}}$. Thus the defining equation for $p_{\mathrm{m,o}}^2/p_{\mathrm{s}}$ will be different for different methods used to obtain the RF modulation of the optical carrier.

1.2.1 The $p_{\mathrm{m,o}}^2/p_{\mathrm{s}}$ of directly modulated laser links

The optical power output of a semiconductor laser is produced from the forward biased current injected into its active region. Figure 1.2 illustrates the instantaneous optical power $p_{\mathrm{L}}(t)$ ($p_{\mathrm{L}}(t) = p_{\mathrm{L}} + p_{\mathrm{l,o}}$) as a function of the total injected current $i_{\mathrm{L}}(t)$, ($i_{\mathrm{L}}(t) = I_{\mathrm{L}} + i_{\mathrm{l}}$). Here, the bias current is I_{L}, and i_{l} is the small-signal RF modulation, i.e., $i_{\mathrm{l}} \ll I_{\mathrm{L}}$. If the modulation current is $\sqrt{2}i_{\mathrm{s}} \cos \omega t$ where i_{s} is the rms magnitude of the RF current, then $p_{\mathrm{l,o}}$ is the rms magnitude of the laser power

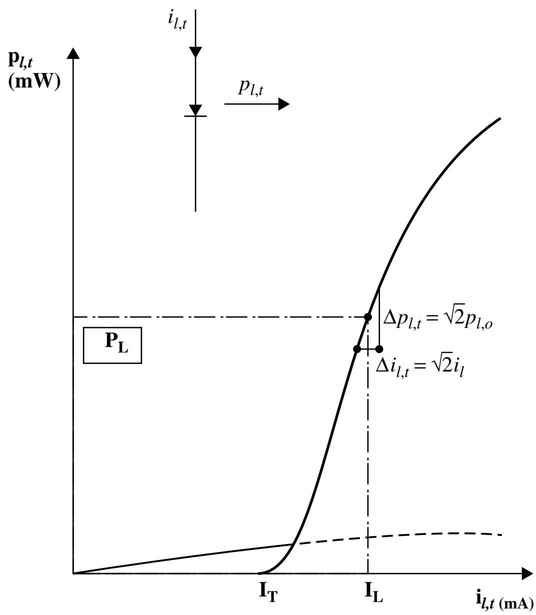

Figure 1.2. Representative plot of a diode laser's optical power, $p_{\mathrm{l,t}}$, vs. the current through the laser, $i_{\mathrm{l,t}}$, with the threshold current, I_{T}, and a typical bias current, i_{L}, for analog modulation.

at ω. Clearly, there is an approximately linear dependence of the change of $p_{\mathrm{L}}(t)$ on the change of $i_{\mathrm{L}}(t)$ in the range from the lasing threshold to the saturation of the laser output.

Direct modulation of semiconductor lasers (i.e., direct modulation of $i_{\mathrm{L}}(t)$) is simpler to implement than external modulation. Hence it is the most commonly used method to achieve intensity modulation of the optical carrier, primarily because it is less expensive. However, the useful bandwidth of modulation is limited to the range from DC to the laser relaxation reasonance, which is typically a few tens of GHz. There is a detailed discussion of the modulation bandwidth, the noise, the nonlinearity, and the modulation efficiency of semiconductor lasers in Chapter 3 of this book.

The slope efficiency of the laser s_{l} is defined as the slope of the $p_{\mathrm{L}}(t)$ vs. $i_{\mathrm{L}}(t)$ curve at a given laser bias current I_{L} in Fig. 1.2,

$$s_{\mathrm{l}} = dp_{\mathrm{L}}(t)/di_{\mathrm{L}}(t)|_{I_{\mathrm{L}}} = p_{\mathrm{l,o}}/i_{\mathrm{l}}. \tag{1.4}$$

Here, s_{l} includes the power coupling efficiency of the laser output to the guided wave mode in the fiber.

The i_{l} is determined from the analysis of the circuit driving the laser. The laser can be represented electrically by an input impedance consisting of a resistance R_{L} in parallel with a capacitance C_{L}.

It is well known in circuit theory that the maximum RF power is transferred from the source at voltage v_{s} to the load impedance when the load impedance is matched to the source impedance, R_{S}. This maximum available power, p_{s}, is $v_{\mathrm{s}}^2/(4R_{\mathrm{S}})$. Therefore the design goal of any RF circuit driving the laser is to provide an impedance match from R_{L} and C_{L} to R_{S}.

Let us consider first a simple resistively matched driving circuit illustrated in Fig. 1.3. This is applicable for frequencies where the reactance of the capacitance, $X_{\mathrm{L}} = 1/j\omega C_{\mathrm{L}} \gg R_{\mathrm{L}}$. For in-plane lasers, typically $R_{\mathrm{S}} \gg R_{\mathrm{L}}$; thus a simple way to satisfy the matching condition at low frequencies is to add a resistance R_{MATCH}

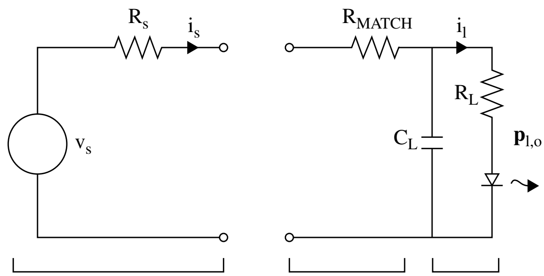

Figure 1.3. Circuit for a resistive magnitude match between a source and a diode laser whose impedance is represented by the parallel connection of a capacitor and a resistor.

in series with the laser so that

$$R_L + R_{MATCH} = R_S. \tag{1.5}$$

Ohm's law permits us to write the expression for the laser current, which in conjunction with Eq. (1.4) yields an expression for the modulated laser power, viz.:

$$i_l = \frac{v_s/2}{(R_L + R_{MATCH})}, \qquad p_{l,o}^2 = \frac{s_l^2}{R_L + R_{MATCH}} \cdot \frac{(v_s/2)^2}{R_s}. \tag{1.6}$$

Dividing the second equation in (1.6) by the maximum power available to the laser at this terminal, p_s, $(v_s/2)^2/R_s$, yields an expression for $p_{l,o}^2/p_s$:

$$\frac{p_{l,o}^2}{p_s} = \frac{s_l^2}{R_s}. \tag{1.7}$$

The frequency variation of $p_{l,o}^2/p_s$ depends on the frequency dependencies of both i_l and s_l. The frequency dependency of s_l will be discussed in Chapter 3; for the purposes of the present discussion it will be assumed to be a constant, independent of frequency.

We can get a feel for the frequency dependency of i_l from the simple circuit of Fig. 1.3. At frequencies higher than DC, i_l drops because of C_L. From the analysis of the circuit shown in Fig. 1.3, we obtain

$$\begin{aligned}
i_s &= \frac{v_s}{R_S + R_{MATCH} + \dfrac{R_L}{1 + R_L(j\omega C_L)}}, \\
i_l &= \frac{i_s}{1 + R_L(j\omega C_L)}, \\
|p_{l,o}| &= s_l|i_l| = s_l v_s \left| \frac{1}{2R_S + (R_S + R_{MATCH})(j\omega C_L)R_L} \right|, \\
\frac{|p_{l,o}|^2}{p_s} &= \frac{s_l^2}{R_S} \left[\frac{1}{1 + \left(2 - \dfrac{R_L}{R_S}\right)^2 \left(\dfrac{R_L \omega C_L}{2}\right)^2} \right].
\end{aligned} \tag{1.8}$$

In addition to the frequency variation of s_l, this matching circuit will cause a 3 dB drop of $|p_{l,o}|^2/p_s$ whenever

$$\frac{R_L \omega C_L}{2} = \frac{1}{2 - \dfrac{R_L}{R_S}}. \tag{1.9}$$

The simple circuit illustrated in Fig. 1.3 may be replaced by any one of a number of more sophisticated circuits that matches R_L and C_L more efficiently to R_S.

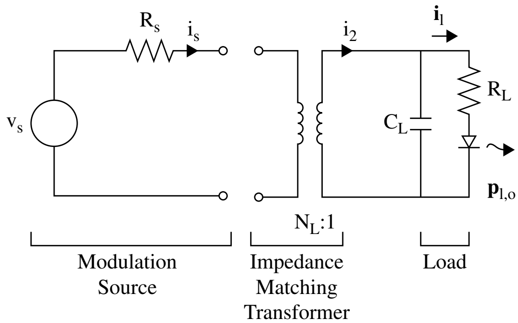

Figure 1.4. Circuit for an ideal transformer magnitude match between a source and a diode laser whose impedance is represented by the parallel connection of a capacitor and a resistor.

Consider here a matching circuit that can be represented symbolically as an ideal transformer as shown in Fig. 1.4. To achieve the desired match, the turns ratio of the transformer is chosen such that

$$N_{\mathrm{L}}^2 R_{\mathrm{L}} = R_{\mathrm{s}}, \qquad \text{and} \quad i_2 = N_{\mathrm{L}} i_{\mathrm{s}}. \tag{1.10}$$

We obtain from conventional circuit analysis:

$$i_{\mathrm{l}} = \frac{v_{\mathrm{s}} N_{\mathrm{L}}}{2R_{\mathrm{s}} + R_{\mathrm{s}} R_{\mathrm{L}}(j\omega C_{\mathrm{L}})},$$

$$\frac{|p_{\mathrm{l,o}}|^2}{p_{\mathrm{s}}} = \frac{s_{\mathrm{l}}^2 N_{\mathrm{l}}^2}{R_{\mathrm{s}}\left[1 + \left(\frac{R_{\mathrm{L}}(\omega C_{\mathrm{L}})}{2}\right)^2\right]}. \tag{1.11}$$

At low frequencies, $j\omega C_{\mathrm{L}}$ is negligible, and we obtain

$$\frac{p_{\mathrm{l,o}}^2}{p_{\mathrm{s}}} = \frac{s_{\mathrm{l}}^2}{R_{\mathrm{s}}} N_{\mathrm{L}}^2. \tag{1.12}$$

Thus transformer (lossless) matching, as show by Eq. (1.12), provides a $p_{\mathrm{l,o}}^2/p_{\mathrm{s}}$ that is N_{L}^2 times larger than the value obtained from resistive (lossy) matching, as shown by Eq. (1.7). The frequency response of this driving circuit will cause a 3 dB drop in $p_{\mathrm{l,o}}^2/p_s$ when

$$\frac{R_{\mathrm{L}}\omega C_{\mathrm{L}}}{2} = 1. \tag{1.13}$$

Comparing Eq. (1.13) with Eq. (1.9), we see that the 3 dB bandwidth of the transformer match is a factor of $2 - \frac{R_{\mathrm{L}}}{R_{\mathrm{s}}}$ larger than for the resistively matched circuit. This is an unusual result in that normally one trades increased response for decreased bandwidth.

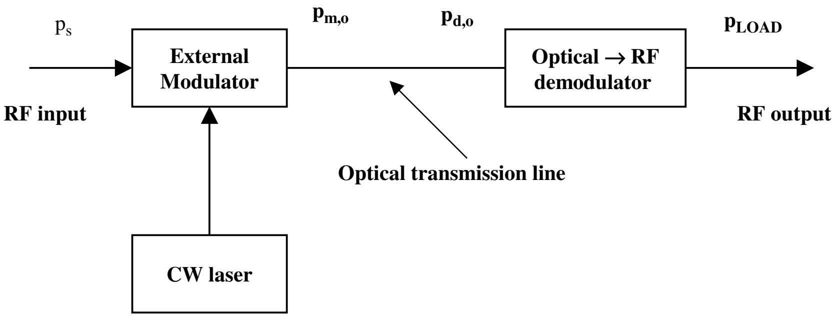

Figure 1.5. Illustration of an externally modulated fiber optic link.

Given the improvement in gain and bandwidth that is obtained in going from a resistive to a transformer match, it is natural to ask: how much further improvement is possible with some other form of matching circuit? Alternatively, one may be interested in using a matching circuit to provide a large i_l, i.e., a large gain g_t, over only a narrow band. The answers to these questions are provided by the Bode–Fano limit. A companion book, *Analog Optical Links*, by Cox [1], also published by Cambridge University Press, discusses such topics extensively.

The discussion in this subsection is applicable to different types of lasers including edge emitting and vertical cavity surface emitting lasers.

1.2.2 The $p^2_{m,o}/p_s$ of external modulation links

For external modulation, the laser operates CW and the desired intensity modulation of the optical carrier is obtained via a modulator connected in series optically with the laser. Figure 1.5 illustrates such an external modulation link. Similar to the case in directly modulated lasers, in external modulation links the frequency variation of $p_{m,o}$ depends on the specific modulator used and on the RF circuit driving the modulator. Different from directly modulated lasers, the bandwidth of state-of-the-art external modulators is approximately five times that of diode lasers. Consequently, the bandwidth of $p^2_{m,o}/p_s$, even when a broadband matching circuit is used, is determined in most applications primarily by the properties of the circuit driving the modulator.

In comparison with directly modulated laser links, the major advantages of external modulation links include (1) the wider bandwidth, (2) higher $p^2_{m,o}/p_s$, (3) lower noise figure and (4) larger *SFDR*. The disadvantages of external modulation links include (1) the additional complexity and cost of optical connections, (2) the necessity of maintaining and matching the optical polarization between the laser and the modulator,[2] and (3) the nonlinear distortions induced by external modulators.

[2] Although polarization independent modulators have been investigated, to date all these modulators have a significant reduction in sensitivity. Thus they are rarely (never?) used in practice.

For more than 10 years the most common type of external modulator that has been considered for RF photonic links is the Mach–Zehnder modulator fabricated in $LiNbO_3$. More recently the polymer Mach–Zehnder modulator as well as the semiconductor Mach–Zehnder and electroabsorption modulators have all also received some consideration for these applications. Each of these modulator types can have one of two types of electrodes: lumped element for lower modulation frequencies and traveling wave for higher frequencies. These different types of modulators are discussed in detail in Chapters 4, 5, 6, and 7 of this book.

The early dominance of the lithium niobate Mach–Zehnder modulator led to the use of the switching voltage for this type of modulator, V_π (to be defined below), as the standard measure of modulator sensitivity. However, with the increasing popularity of alternative types of external modulators – primary among them at present is the electroabsorption (EA) modulator – there is the need to compare the effectiveness of completely different types of modulators. Further, there is also the issue of how to compare the effectiveness of external modulation with direct.

One way to meet these needs, that has proved quite useful from a link perspective, is to extend the concept of slope efficiency – discussed above for direct modulation – to external modulation. This is readily done by starting with the external modulator transfer function, which is often represented in the literature by an optical transmission T of the CW laser power as a function of the voltage ν_{M} across the modulator, $T(\nu_{\mathrm{M}})$. To incorporate $T(\nu_{\mathrm{M}})$ into the external modulation slope efficiency we need two changes in units: modulation voltage to current and optical transmission to power. When these conversions are substituted into Eq. (1.4) we obtain

$$s_{\mathrm{m}} \stackrel{\Delta}{=} \left.\frac{dp(i_{\mathrm{L}})}{di_{\mathrm{L}}}\right|_{I_{\mathrm{M}}} = R\left.\frac{dp(i_{\mathrm{L}})}{d\nu_{\mathrm{M}}}\right|_{V_{\mathrm{M}}} = RP_{\mathrm{L}}\left.\frac{dT(\nu_{\mathrm{M}})}{d\nu_{\mathrm{M}}}\right|_{V_{\mathrm{M}}}. \tag{1.14}$$

Here R is the modulator impedance, P_{L} is the CW laser power at the input to the modulator and V_{M} is the modulator bias point.

Let us assume first that, within a given bandwidth of ω, T responds instantaneously to ν_{M}. In other words, T is a function of the instantaneous V, independent of the time variation of ν_{M} (this compares to the lumped element electrode case). For example, in Mach–Zehnder modulators whether fabricated in $LiNbO_3$ or polymers, it is well known that

$$T = \frac{T_{\mathrm{FF}}}{2}\left[1 + \cos\left(\frac{\pi\,\nu_{\mathrm{M}}}{V_\pi}\right)\right], \tag{1.15}$$

where T_{FF} is the fraction of the total laser power in the modulator input fiber that is coupled into the modulator output fiber when the modulator is biased for maximum transmission. In a balanced modulator, one of the transmission maxima occurs

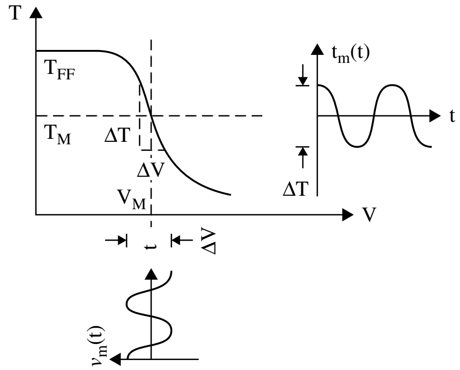

Figure 1.6. Illustration of the transmission T of an external modulator as a function of V. The $V(t)$ is illustrated in the inset below the $T(V)$ curve. It consists of the bias voltage V_M and the RF voltage $\nu_m(t)$. The transmittance T as a function of t is shown in the inset on the right. It consists of a bias transmittance T_M and a time varying transmittance $t_m(t)$.

at $\nu_M = 0$. V_π is the value of ν_M which is required to shift the modulator from maximum to minimum transmission; ideally, at minimum transmission $T = 0$. In electroabsorption modulators,

$$T = T_{FF}e^{-\alpha(\nu_M)L}. \tag{1.16}$$

Here, L is the length of the modulator, and α is the absorption coefficient.

The relationship between T and ν_M is illustrated in Fig. 1.6. At $\nu_M = V_M$, the bias transmission is T_M. The total applied voltage ν_M consists of the sum of a DC bias V_M and a RF voltage $\nu_m(t)$. For a single frequency RF input, $\nu_M(t) = V_M + \nu_m(t)$ and $\nu_m(t) = \sqrt{2}\nu_{rf}\cos\omega t$, where ν_{rf} is the rms RF voltage applied to the modulator. The resultant T is $T(t) = T_M + t_m(t)$. The resultant $t_m(t)$ and the input $\nu_m(t)$ as a function of time are illustrated in the two inset figures on the right hand side and below the $T(V)$ figure. The optical carrier power in the optical fiber transmission line, immediately after the modulator, is $P_L T$, where $P_L T = P_L T_M + P_L t_m(t)$. In general, T is not a linear function of ν_M, and t_m is a distorted $\cos\omega t$ function.

As seen by Eqs. (1.15) and (1.16), we often have an analytic expression of $T(\nu_M)$ for an external modulator. In such cases, in the small-signal approximation ($\nu_m \ll V_M$), T can be expressed as a Taylor series expansion with $(\nu_m\cos\omega t)^n$ terms. The higher order terms give rise to distortions to the modulating signal and will be discussed again in Section 1.4.

In the first-order approximation (neglecting $n > 1$ terms), we can apply Eq. (1.15) to Eq. (1.14) to yield an expression for the slope efficiency of Mach–Zehnder modulators,

$$s_m = -\frac{\pi T_{FF} P_L R}{2V_\pi}. \tag{1.17}$$

Applying Eq. (1.16) to Eq. (1.14) yields the analogous expression for electroabsorption modulators,

$$s_m = -\frac{\pi T_{FF} P_L R}{2V_{\pi,eq}}, \tag{1.18}$$

where $V_{\pi,eq}$ is defined in Chapter 6.

From Eqs. (1.17) and (1.18), it is clear that to increase the slope efficiency, one wants a low value of V_π; in other words one wants as sensitive a modulator as possible. It is also clear from these equations that to maximize the slope efficiency it is equally important to have the product of the average optical power and the optical transmission as high as possible. Thus one wants a modulator with as little optical loss as possible and a laser with as high optical power as feasible.

It is important to note that all three of these parameters – V_π, T_{FF} and P_L – can be chosen independently. Therefore the upper bound on s_m for external modulation is not set by fundamental limits but by practical considerations. This is in contradistinction to the direct modulation case where there is a fixed upper bound to these quantities that is set by conservation of energy.

At high frequencies, T is no longer just a function of V. T depends on the time variation of the RF signal. In other words s_m is dependent on ω. This case corresponds to traveling wave modulators, two examples of which will be discussed in Chapters 5 and 6.

Similar to the case for directly modulated lasers, in external modulation links the frequency dependence of $p_{m,o}$ is a product of the frequency dependence of s_m and ν_m. Both the magnitude (e.g., T_{FF} and V_π, or $V_{\pi,eq}$) and the frequency dependence of s_m will be different for different types of modulators such as the $LiNbO_3$ and polymer Mach–Zehnder modulators and electroabsorption modulators, and for different electrode designs such as lumped element and traveling wave. The s_m properties of various modulators will be discussed in Chapters 4 to 7. In the remaining discussion of this subsection we will assume s_m to be independent of ω.

It is important to note that s_m and the bandwidth of the modulator cannot be optimized independently. The V_π or $V_{\pi,eq}$, i.e., s_m, is directly related to the C_M of the modulator. For example, in a lumped element Mach–Zehnder modulator V_π is inversely proportional to the length of the electrode L, while C_M is proportional to L. Therefore there is a direct trade-off between s_m and the bandwidth of $p_{m,o}^2/p_s$. The trade-off between s_m and the bandwidth for electroabsorption modulators is discussed in Chapter 6. The common practice for broadband applications is to determine the largest C_M that will provide the desired bandwidth and then design the modulator electrodes, i.e., L, to maximize s_m under that constraint.

As was the case with matching to the diode laser, the magnitude and the frequency dependence of ν_m will depend on the modulator input impedance, the driving circuit design, and the modulator electrode configuration – lumped element or traveling wave. Further, the matching circuit design approach will be the same as for the direct modulation case, however the details will be different because external modulators are voltage controlled devices with high input impedance while the lasers are current controlled devices with low input impedance.

1.2.2.1 Impedance matching to lumped element modulators

In all lumped element external modulators, v_{m}, the time dependent voltage across the waveguide, is considered to be independent of the position along the electrode. Electrically, the modulator electrode behaves like a lumped capacitor in parallel with a leakage resistance. Although more sophisticated representation of some modulators may include additional resistance or reactance, we will base our discussion here on an equivalent circuit of a capacitance C_{M} in parallel with a resistance R_{M}. In comparison, the equivalent circuit for forward biased diode lasers has a small R_{L}, whereas here R_{M} is a high resistance.

As we did for the diode laser, we will present expressions for $p^2_{\mathrm{m,o}}/p_{\mathrm{s}}$ with resistive and transformer type impedance matches to the modulator. Figure 1.7 shows a circuit using a resistance R_{MATCH} for matching. Since $R_{\mathrm{M}} \gg R_{\mathrm{S}}$, R_{MATCH} is placed in parallel with R_{M}. From circuit analysis, we obtain

$$v_{\mathrm{m}} = v_{\mathrm{s}} \frac{\left(\dfrac{R_{\mathrm{E}}}{R_{\mathrm{E}} + R_{\mathrm{S}}}\right)}{1 + \dfrac{R_{\mathrm{S}} R_{\mathrm{E}}}{R_{\mathrm{S}} + R_{\mathrm{E}}}(j\omega C_{\mathrm{M}})}, \qquad \text{where } R_{\mathrm{E}} = \frac{R_{\mathrm{M}} R_{\mathrm{MATCH}}}{R_{\mathrm{M}} + R_{\mathrm{MATCH}}}. \quad (1.19)$$

For maximum transfer of RF power at low ω, R_{E} is designed to be equal to R_{S}.

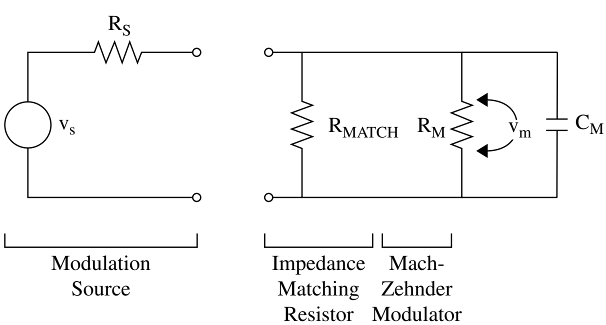

Figure 1.7. Circuit of a resistive magnitude match between a resistive source and the parallel connection of two lumped elements – R and C – which represent a first order impedance model for a Mach–Zehnder or an electroabsorption modulator.

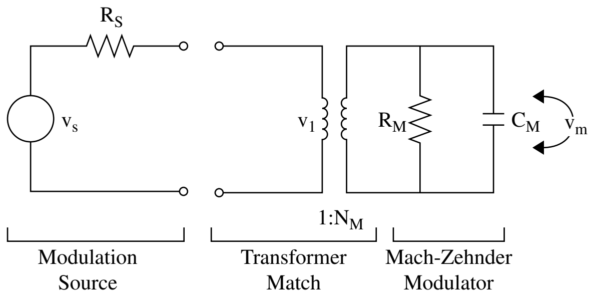

Figure 1.8. Circuit for an ideal transformer magnitude match between a source and the *RC* impedance model for a Mach–Zehnder or an electroabsorption modulator.

Therefore,

$$\frac{p_{\mathrm{m,o}}^2}{p_{\mathrm{S}}} = \frac{s_{\mathrm{m}}^2}{R_{\mathrm{S}}} \frac{1}{1 + (\omega C_{\mathrm{M}} R_{\mathrm{S}}/2)^2}. \tag{1.20}$$

Higher efficiency matching can again be obtained using a lossless circuit that can be represented as a transformer matching the input impedance to R_{S}. Figure 1.8 illustrates the use of an ideal transformer to match the input impedance of a modulator to R_{S}. Since $R_{\mathrm{M}} > R_{\mathrm{S}}$, we need a step-up transformer for matching, with $N_{\mathrm{M}}^2 R_{\mathrm{S}} = R_{\mathrm{M}}$ and $v_{\mathrm{m}} = N_{\mathrm{M}} v_1$. From the circuit analysis we obtain

$$v_{\mathrm{m}} = N_{\mathrm{M}} v_{\mathrm{s}} \frac{R_{\mathrm{M}}}{\left(R_{\mathrm{M}} + N_{\mathrm{m}}^2 R_{\mathrm{S}}\right) + N_{\mathrm{m}}^2 R_{\mathrm{S}} R_{\mathrm{M}} (j\omega C_{\mathrm{M}})} = N_{\mathrm{M}} v_{\mathrm{S}} \frac{1/2}{1 + [N_{\mathrm{M}} R_{\mathrm{M}} (j\omega C_{\mathrm{M}})/2]}$$

and

$$\frac{p_{\mathrm{m,o}}^2}{p_{\mathrm{s}}} = \frac{s_{\mathrm{m}}^2 N_{\mathrm{M}}^2}{R_{\mathrm{S}}} \frac{1}{1 + \left(\dfrac{N_{\mathrm{M}}^2 \omega R_{\mathrm{S}} C_{\mathrm{M}}}{2}\right)^2}. \tag{1.21}$$

Comparing Eq. (1.20) with Eq. (1.21), we conclude that the transformer matching yields a low frequency gain that is N_{M}^2 times larger than the resistive matching. However we also note that the transformer match bandwidth is N_{M}^2 lower than the resistor match bandwidth. This represents the more typical situation where the gain increases by the same factor that the bandwidth decreases such that the gain–bandwidth product remains constant.

1.2.2.2 Impedance matching to traveling wave modulators

In Chapters 5 and 6, it will be shown that the electrodes of traveling wave modulators form an electrical transmission line. When the electrical propagation loss is negligible, the transmission line has a real characteristic impedance Z_0 which is independent of ω. The transmission line is usually terminated with a load resistance

R_L, where $R_L = R_0$ so that the input equivalent impedance of the terminated modulator is just a pure resistance R_0. In this case, the results obtained in Eqs. (1.19) to (1.21) are applicable, except that $C_M = 0$ under this condition. The equations predict and infinitely wide bandwidth. If $R_0 = R_S$(R_S is usually 50 ohms), we have an ideal match to the modulation source without the use of any matching circuit. Although it is desirable to design Z_0 to be close to R_S from the impedance matching point of view, Z_0 is often considerably lower than R_S to obtain a large s_m. The trade-offs between s_m and Z_0 for Mach–Zehnder and electroabsorption modulators are discussed in Chapters 5 and 6. In reality, if Z_0 is significantly different than R_S, it is difficult to obtain a broadband match.

1.2.3 The $p_l/p_{d,o}^2$ of photodetectors

The photodiode generates an RF current i_d which is proportional to the optical power at the frequency ω incident on the photodiode, $p_{d,o}$. In other words, $i_d = s_d p_{d,o}$, where s_d is the slope efficiency of the photodiode in units of A/W. Let the photodiode be represented electrically by R, C_D, and R_D, as shown in Fig. 1.9. R is the leakage resistance of the reverse biased photodiode. It is typically very large compared to R_D and R_{LOAD}. The RF output power from the photodiode is delivered to the load shown as R_{LOAD}, where $R_{LOAD} > R_D$. To maximize the power transferred to the load, we need to match R, C_D, and R_D, to R_{LOAD}.

As an example, we have chosen the transformer matching circuit shown in Fig. 1.9. In this case,

$$i_{LOAD} = N_D i_2,$$
$$i_{LOAD} = \frac{N_D}{\left(R_D + N_D^2 R_{LOAD}\right)(j\omega C_D) + 1 + \dfrac{R_D + N_D^2 R_{LOAD}}{R}} i_d. \tag{1.22}$$

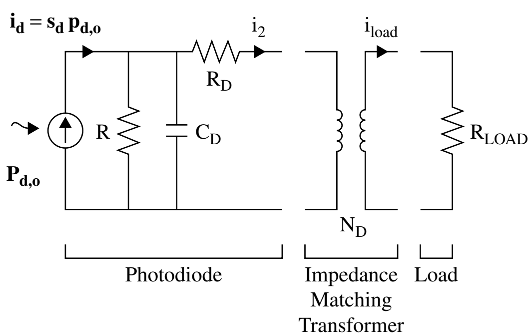

Figure 1.9. Schematic of simple, low frequency photodiode circuit model connected to an ideal transformer for magnitude matching the photodiode to a resistive load.

For a practical transformer turns ratio, $N_D^2 R_{LOAD}$ cannot match R. Thus $R \gg R_D + N_D^2 R_{LOAD}$, and we obtain:

$$\frac{p_l}{p_{d,o}^2} = \frac{i_{LOAD}^2 R_{LOAD}}{(i_d/s_d)^2} = \frac{N_D^2 s_d^2 R_{LOAD}}{\left(R_D + N_D^2 R_{LOAD}\right)^2 \omega^2 C_D^2 + 1}. \tag{1.23}$$

Equation (1.23) allows us to explore the changes in gain and bandwidth as a function of N_D. Let us assume that s_d is independent of ω within the frequency range of interest, then

$$\text{Gain increase}|_{\text{low}\,\omega} = \left.\frac{p_l}{p_{d,o}^2}\right|_{N_D} \Big/ \left.\frac{p_l}{p_{d,o}^2}\right|_{N_D=1} \cong N_D^2. \tag{1.24}$$

$$\text{Bandwidth increase} = \frac{R_D + R_{LOAD}}{R_D + N_D^2 R_{LOAD}} \cong \frac{1}{N_D^2}. \tag{1.25}$$

Equations (1.25) and (1.26) express the same result we obtained for the modulator, that the product of gain and bandwidth is a constant. Consequently detector circuits (i.e., the N_D) can be designed to provide the highest gain within a desired bandwidth.

In reality the slope efficiency s_d also has a bandwidth dependence. Detectors with large s_d have generally small bandwidth. Figure 1.10 shows the slope efficiency of some commonly used photodetectors versus the 3 dB frequency. Chapter 8 discusses in detail the s_d for various photodetectors.

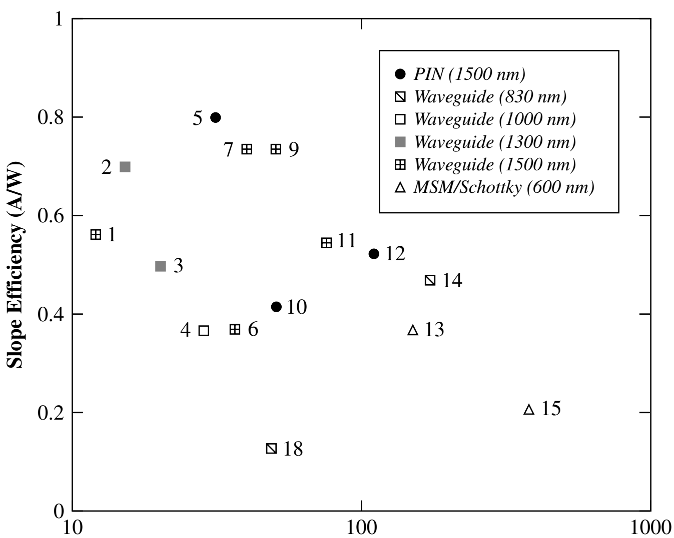

Figure 1.10. Plot of photodetector slope efficiency vs. upper 3 dB frequency for various photodetectors.

1.2.4 General comments on link gain

We can now combine the specific expressions of the previous sections into the general expression for link gain, Eq. (1.3a). For the low frequency gain of a direct modulation link we insert Eqs. (1.12) and (1.23) – the latter with $\omega \rightarrow 0$ – into Eq. (1.3a) to obtain:

$$g_{\text{t-DM}} = \frac{N_{\text{L}}^2 s_{\text{l}}^2}{R_{\text{S}}} s_{\text{d}}^2 N_{\text{D}}^2 R_{\text{LOAD}} = s_{\text{l}}^2 s_{\text{d}}^2 \big|_{R_{\text{S}}=R_{\text{LOAD}};N_{\text{L}}=N_{\text{D}}=1} \tag{1.26a}$$

The analogous expression for an external modulation link is obtained by substituting Eqs. (1.20) and (1.23) into Eq. (1.3a). We continue to assume that $\omega = 0$ in Eqs. (1.21) and (1.23). The result is

$$g_{\text{t-DM}} = \frac{N_{\text{M}}^2 s_{\text{m}}^2}{R_{\text{S}}} s_{\text{d}}^2 N_{\text{D}}^2 R_{\text{LOAD}} = s_{\text{m}}^2 s_{\text{d}}^2 \big|_{R_{\text{S}}=R_{\text{LOAD}};N_{\text{M}}=N_{\text{D}}=1} \tag{1.26b}$$

In comparing Eqs. (1.26a) and (1.26b) we see one of the advantages of expressing the link gain in terms of slope efficiency: a simple expression which can be applied to both types of modulations.

In all early links – and most links today – $g_{\text{t}} < 1$, which means the links have loss. This is consistent with the fact that the slope efficiencies of conventional diode lasers and PIN photodetectors are constrained by energy conservation to be < 1. By inference, it was assumed that the slope efficiency of external modulators was also constrained to be < 1.

There are two general approaches to reducing the link loss, which may be used separately or in conjunction. For narrow band links, it is possible to trade excess bandwidth for reduced loss. To achieve gain in a directly modulated link, for example, requires $R_{\text{D}}/R_{\text{L}} > s_{\text{l}}^2 s_{\text{d}}^2$. This has been demonstrated experimentally by Ackerman *et al.* [2]. The Bode–Fano limit defines the extent of this trade-off [3].

The other general approach to reduce the link loss is to increase the slope efficiency. This is a broadband approach that does not involve a gain–bandwidth trade-off. Although in principal it would be equally effective to improve the slope efficiency of either the modulation device or the photodetector, in practice all attention has focused on improving the modulation device.

The first theoretical study – and experimental verification – of improved slope efficiency was by Cox et al. [4] for external modulation. This work demonstrated a slope efficiency of 2.2 W/A and a net link power gain of 1 dB out to 150 MHz. More recently Williams *et al.* [5] have applied this technique to produce an external modulation link with 3 dB gain over 3 GHz.

It is also possible to improve the broadband slope efficiency of direct modulation. One technique for doing so is the cascade laser – as proposed and demonstrated by Cox *et al.* [6]. Using discrete devices, a link gain of 3.8 dB has been achieved over a bandwidth of < 100 MHz. Further improvements are anticipated as integrated versions are developed.

1.3 Noise figure

Noise plays important roles in setting the minimum magnitude signal that can be conveyed by the link and in contributing to the maximum *SFDR* for RF photonic links. The *SFDR* of RF photonic links will be discussed in detail in Section 1.4. We will focus our discussion in this section on noise sources and the noise figure.

For RF photonic links the noise power at the output of the link n_{out} is related to the noise at the input of the link n_{in} by the noise figure, *NF*, which is defined as,

$$NF = 10\log_{10}\left(\frac{s_{\text{in}}/n_{\text{in}}}{s_{\text{out}}/n_{\text{out}}}\right) = 10\log_{10}\left(\frac{n_{\text{out}}}{g_{\text{t}}n_{\text{in}}}\right),$$
$$\text{where} \quad n_{\text{in}} = kT_{\text{o}}\Delta f \quad \text{and} \quad T_{\text{o}} = 290\,\text{K}. \tag{1.27}$$

Here, s_{in} and s_{out} are the RF signal power at frequency ω at the input and the output of the link, respectively, k is Boltzmann's constant and Δf is the noise bandwidth. When the input and output terminals are matched, $s_{\text{out}}/s_{\text{in}}$ is the gain of the link g_{t}, which we learned how to analyze in the previous section.

The two forms of Eq. (1.27) make clear a couple of facts about the noise figure: (1) when there is no noise added by the link, the minimum *NF* is 0 dB, and (2) *NF* does not depend on the signal power s_{in}.

Clearly, n_{out} will be larger than $g_{\text{t}}n_{\text{in}}$ because of the additional noise contributions from the laser, the detector and the circuit elements. Therefore, we can rewrite Eq. (1.27) as

$$n_{\text{out}} = g_{\text{t}}n_{\text{in}} + n_{\text{add}} \text{ and } NF = 10\log_{10}\left(1 + \frac{n_{\text{add}}}{g_{\text{t}}n_{\text{in}}}\right). \tag{1.28}$$

From an alternative point of view, the effect of additional noise n_{add} in Eq. (1.28) can be considered as an equivalent additional noise at the input which is $n_{\text{add}}/g_{\text{t}}$. Equation (1.28) can also be generalized to include noise added at any point in the link $n_{\text{add},i}$,

$$NF = 10\log_{10}\left(1 + \frac{\sum_i n_{\text{add},i}/g_i}{n_{\text{in}}}\right). \tag{1.29}$$

Here g_{i} is the gain between the link input and the additional noise source.

NF is commonly used to specify the noise property of any RF component. Equations (1.27) and (1.28) allow us to express n_{out} in terms of the NF of the link when $n_{\text{in}} = kT_{\text{o}}\Delta f$. The primary objective of this section is to discuss how to find the *NF* of a link.

1.3.1 Noise sources and their models

There are three dominant noise sources in photonic links: thermal, shot and relative intensity noise. All noise sources are statistically independent, so the total noise power from all these sources is simply the sum of the independent noise powers. In the following subsections, we will show the mean square current representation of these noise sources.

1.3.1.1 Thermal noise

Whenever any resistor is used in a circuit, it generates thermal noise, which is also known as the Johnson noise. It is a white noise, meaning that the noise power per unit bandwidth is a constant, independent of the frequency. To limit the noise power contributed by such a broadband noise source, there is usually an electrical filter of bandwidth Δf put in the circuit. Only the signals and the noise within this band need to be considered in the link. The noise contributed by a physical resistance R is commonly treated as a mean square current noise generator in parallel with a noise-free resistor R. The mean square noise current of the thermal noise is

$$\overline{i_{\mathrm{t}}^2} = \frac{4kT\Delta f}{R}, \tag{1.30}$$

where, T is the temperature in kelvin. For each mean squared current representation, it is well known in circuit theory that there is also an equivalent mean squared voltage representation of the same noise source. Figure 1.11 shows that, for terminals A and B, a $\overline{v_{\mathrm{noise}}^2}$ in series with R is completely equivalent to the $\overline{i_{\mathrm{noise}}^2}$ in parallel with R, provided $\overline{v_{\mathrm{noise}}^2} = R^2\overline{i_{\mathrm{noise}}^2}$.

For any complex impedance, thermal noise is generated in the resistive part of the impedance. When there is a load matched to R, the noise power delivered to the load is $(\overline{i_{\mathrm{t}}^2}/4)R = kT\Delta f$.

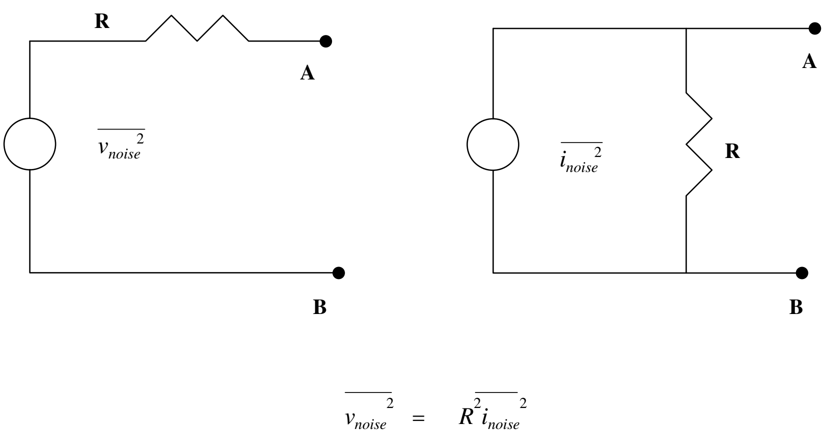

Figure 1.11. The equivalent mean squared voltage and current source of noise.

1.3.1.2 Shot noise

Shot noise is generated whenever an electrical current with average value $\overline{I_D}$ is generated via a series of independent random events, e.g. the photocurrent in a detector. Shot noise is also a white noise source. Within a filter bandwidth Δf, the shot noise is represented by a mean square shot noise current generator (placed in parallel with a noiseless current generator I_D),

$$\overline{i_{sn}^2} = 2q\overline{I_D}\Delta f, \tag{1.31}$$

where q is the charge of an electron. Note that the shot noise is linearly proportional to I_D. Thus the shot noise can be larger than the thermal noise for sufficiently large I_D. It represents one of the disadvantages of using large P_L in photonic links. For example, the shot noise at 1 mA of I_D is equal to the thermal noise of a 50 ohm resistor at room temperature (290 K).

1.3.1.3 Relative intensity noise

There are fluctuations of laser intensity caused by random spontaneous emissions. These fluctuations are known as the relative intensity noise (*rin*). The *rin* is defined as

$$rin = \frac{\overline{\delta p_I^2}\Delta f}{\overline{P_L^2}}. \tag{1.32}$$

Here $\overline{\delta p_I^2}$ denotes the mean of the squared spectral density intensity fluctuations, and $\overline{P_L^2}$ is the average laser power squared. In general *rin* is a function of $\overline{P_L^2}$. It reaches maximum just above the lasing threshold and it decreases as the laser is above threshold. Relative intensity noise of a laser is usually specified in terms of *RIN*. *RIN* is related to *rin* by

$$RIN = 10\log_{10}(rin). \tag{1.33}$$

The *RIN* spectrum is not flat and hence this is not a white noise source. However, for simplicity, most link analyses assume that *RIN* is a constant within the bandwidth of interest. *RIN* also differs for diode and solid state lasers, and for single mode and multimode lasers. For example, single mode solid state lasers may have a *RIN* of -170 dB for $\Delta f = 1$ Hz, whereas diode lasers typically have a *RIN* of -145 dB for $\Delta f = 1$ Hz.

Both the $\overline{P_L^2}$ and the $\overline{\delta p_I^2}$ will produce corresponding currents squared in the load resistor after detection. Since the same detector and circuit will be used for $\overline{P_L^2}$ and $\overline{\delta p_I^2}$, the ratio of $\overline{\delta p_I^2}/\overline{P_L^2}$ is the same as $\overline{i_{rin}^2}/\overline{I_D}^2$. Hence the relative intensity noise can be represented as a current generator with a mean square current as

$$\overline{i_{rin}^2} = rin \cdot \overline{I_D}^2 \cdot \Delta f. \tag{1.34}$$

Notice that $\overline{i^2_{rin}}$ is proportional to $\overline{I_{\mathrm{D}}}^2$, whereas the shot noise is only linearly proportional to I_{D}. Therefore the *RIN* noise dominates at high laser average power.

1.3.2 Noise figure analysis of representative links

To find the noise figure of a link, we need to calculate either the n_{add} at the output or the equivalent noise at the input, $\Sigma n_{\mathrm{i,add}}/g_{\mathrm{i}}$. In Figs. 1.3, 1.4, 1.7 and 1.8, we have shown examples of the circuit for the RF source driving the laser or the modulator. In Fig. 1.9 we have shown an example of the circuit in which the photodetector is matched to the load. In all links for the transmission of RF, the $p_{\mathrm{d,o}}$ input to the photodetector is proportional to $p_{\mathrm{m,o}}$, i.e., the modulated output of the modulation device. If we now add mean square noise current generators at various locations of the elements (such as the laser, the detector, and the resistance, that generate the noise) to the driving and detector circuits, we can calculate the resultant n_{add} or the $\Sigma n_{\mathrm{i,add}}/g_{\mathrm{i}}$ from circuit analysis. In such a calculation, all circuit elements, except the noise sources, will be considered noiseless elements.

Clearly, the *NF* of a given link will depend on the noise sources, their locations and the circuit configuration of the link. Fortunately, when the n_{add} is caused primarily by a dominant noise source, other noise sources can be neglected. Whether the dominant noise mechanism is thermal, shot or *RIN* noise will depend both on the operating conditions – such as the bias laser power and the average detector current – and on the circuit. We will now discuss how to calculate the *NF* for two cases that occur frequently.

1.3.2.1 *The* NF *of a* RIN *noise dominated link using a directly modulated laser*

Figure 1.12 shows the equivalent circuits of a transformer matched directly modulated laser link including the noise sources, which is based on the laser and detector circuits without the noise sources that have been shown in Fig. 1.4 and Fig. 1.9. For the convenience of calculation, the thermal noises due to the resistances R_{S} and R_{L} are represented by the equivalent noise voltage source in series with the resistance. The *RIN* noise is shown as a current noise source in parallel with the photodetector:

$$\begin{aligned} \overline{v^2_{\mathrm{ts}}} &= 4kTR_{\mathrm{s}}\Delta f, \qquad \overline{v^2_{\mathrm{ti}}} = 4kTR_{\mathrm{L}}\Delta f,\\ \overline{i^2_{\mathrm{tLOAD}}} &= 4kT\Delta f/R_{\mathrm{L}}, \qquad \overline{i^2_{rin}} = rin\overline{I_{\mathrm{D}}}^2\Delta f. \end{aligned} \tag{1.35}$$

The *RIN* of a typical diode laser is < -150 dB/Hz and the average detector current is 1 mA. Under these assumptions $\overline{i^2_{rin}} = 1.0 \times 10^{-21} > \overline{i^2_{\mathrm{sn}}} = i^2_{\mathrm{t}} = 3.2 \times 10^{-22}$ A^2/Hz. Consequently we can obtain a reasonably accurate value for the *NF* based on only two contributions to n_{add}. One is the thermal noise of R_{L}. Since the

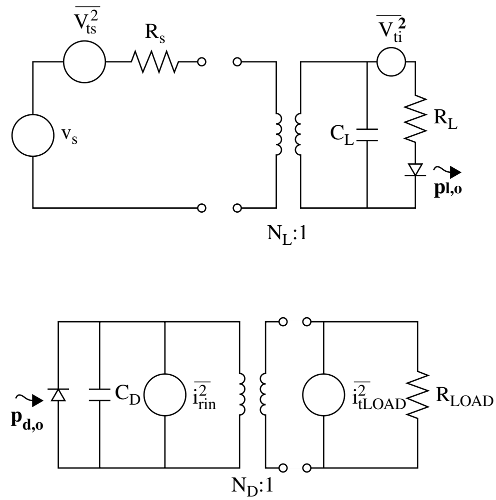

Figure 1.12. The equivalent circuit of a RF link for *NF* calculation with *RIN* dominated noise and a directly modulated laser.

noise source is located in the same loop as the modulation source, it is easy to verify that this source has the same gain from input to output as the modulation source. Therefore, its contribution to n_{add} is $g_t kT\Delta f$. The other contribution to n_{add} is the *RIN* noise. Since it is located at the link output before the transformer, its contribution to n_{add} can be written by inspection to be $N_{\text{D}}^2 \overline{i_{rin}^2} R_{\text{LOAD}} \Delta f$.

Consequently, we obtain

$$NF = 10\log_{10}\left(1 + \frac{g_t kT + \overline{i_{rin}^2} N_{\text{D}}^2 R_{\text{LOAD}}}{g_t kT}\right) = 10\log_{10}\left(2 + \frac{\overline{i_{rin}^2} R_{\text{LOAD}}}{N_1^2 s_1^2 s_d^2 kT}\right). \tag{1.36}$$

Figure 1.13 is a plot of Eq. (1.36) with $s_1 = 0.2$ W/A, $s_d = 0.8$ A/W, $T = 290$ K, and $R_{\text{LOAD}} = 50\ \Omega$. It confirms our intuition that as the *RIN* increases so does the *NF*. For an $\overline{I_{\text{D}}}$ of 1 mA, the shot noise would be equal to the *RIN* noise at -168 dBm. Therefore the link would be shot noise dominated for *RIN* less than -168 dBm. and the above analysis would need to be modified. Notice also that, even for every small *RIN* and shot noise, the *NF* never decreases below 3 dB [$= 10\log_{10}(2)$]. The theoretical limit of the noise figure for any RF photonic link with passive matching at the input is discussed in more detail in Section 1.3.3.

1.3.2.2 The NF *of a shot noise dominated link using an external modulator*

Figure 1.14 shows the equivalent circuit for calculating the *NF* of a RF link dominated by shot noise and using an external modulator. Solid state lasers, which typically have RIN < -175 dB/Hz, have often been used as the CW source for

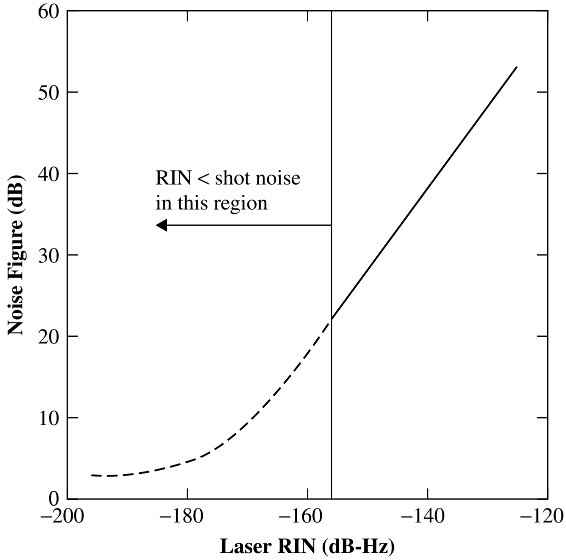

Figure 1.13. Plot of the *NF* of a *RIN* dominated directly modulated laser RF link as a function of *RIN*.

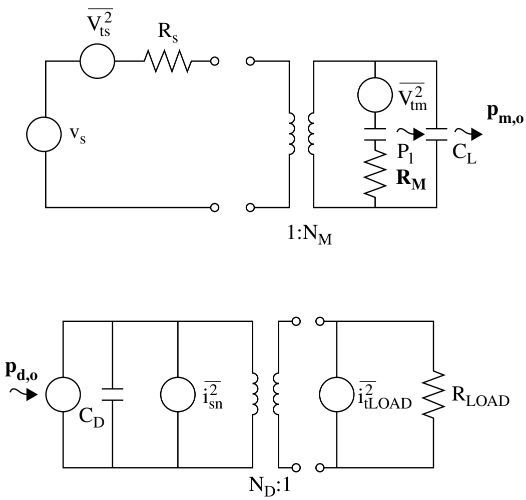

Figure 1.14. The equivalent circuit of an RF link for *NF* calculation with external modulator, dominated by shot noise.

external modulation. The typical $\overline{P_L} = 10$ mW and $T_{FF} = 3$ dB, resulting in an $\overline{I_D} = 4$ mA (for $s_d = 0.8$ A/W). Consequently,

$$i^2_{sn} = 1.28 \times 10^{-21}\ \text{A}^2/\text{Hz} > i^2_t = 3.20 \times 10^{-22}\ \text{A}^2/\text{Hz (for } R = 50\,\Omega) \\ > i^2_{rin} = 5.06 \times 10^{-23}\ \text{A}^2/\text{Hz}. \tag{1.37}$$